

## Rotation-induced grain growth and stagnation in phase-field crystal models

Mathias Bjerre,<sup>1</sup> Jens M. Tarp,<sup>1</sup> Luiza Angheluta,<sup>2</sup> and Joachim Mathiesen<sup>1</sup>

<sup>1</sup>*Niels Bohr Institute, University of Copenhagen, Blegdamsvej 17, DK-2100 Copenhagen, Denmark*

<sup>2</sup>*Physics of Geological Processes, Department of Physics, University of Oslo, Oslo, Norway*

(Received 27 May 2013; published 15 August 2013)

We consider grain growth and stagnation in polycrystalline microstructures. From the phase-field crystal modeling of the coarsening dynamics, we identify a transition from a grain-growth stagnation upon deep quenching below the melting temperature  $T_m$  to a continuous coarsening at shallower quenching near  $T_m$ . The grain evolution is mediated by local grain rotations. In the deep quenching regime, the grain assembly typically reaches a metastable state where the kinetic barrier for recrystallization across boundaries is too large and grain rotation with subsequent coalescence or boundary motion is infeasible. For quenching near  $T_m$ , we find that the grain growth depends on the average rate of grain rotation, and follows a power-law behavior with time, with a scaling exponent that depends on the quenching depth.

DOI: [10.1103/PhysRevE.88.020401](https://doi.org/10.1103/PhysRevE.88.020401)

PACS number(s): 81.10.-h, 64.60.Cn, 05.70.Ln, 05.70.Np

*Introduction.* Polycrystalline microstructures are typically formed by thermal processes such as quenching or annealing of melts, through the nucleation and growth of grains of different crystallographic orientation. Since these microstructures have a controlling role on the large scale material properties, e.g., mechanical, magnetic, and optical properties, and yield strength, it is crucial to understand their formation and late-stage evolution.

Curvature-driven grain growth is described in two dimensions (2D) by the von Neumann–Mullins growth law and predicts a linear growth of the average grain area  $\langle A \rangle \sim t$  that follows directly from the linear relationship between grain-boundary normal velocity and curvature [1,2]. However, one common intriguing finding in experiments with thin metallic films and molecular dynamics simulations of annealed polycrystalline systems is that the coarsening deviates substantially from the curvature-driven growth [3,4]. Instead, the grain area size increases as  $\langle A \rangle \sim t^\alpha$ , where the value of the scaling exponent  $\alpha$  may depend nontrivially on a number of controlling factors, such as the annealing temperature, grain size, grain-boundary mobility, and surface energy. For instance, the growth kinetics in nanocrystalline Fe was experimentally observed to be controlled by the grain size, leading to a superdiffusive growth,  $\alpha \approx 2$  [5]. However, at mesoscales, the coarsening law in metallic thin films is typically subdiffusive,  $\alpha \approx 1/2$  [6,7]. A unified theoretical foundation for the anomalous grain growth is still lacking, despite numerous attempts to generalize the phenomenological normal growth model to include additional mechanisms that control the growth rate [8,9].

Grain-growth stagnation is another anomalous behavior to the classical picture of a curvature-driven scaling law that occurs in a wide range of materials ranging from metallic thin films [7,10] to ice [11]. Although the thermodynamically stable state consists of a single crystal, the kinetics towards equilibrium goes through an energy landscape with possible metastable states where grain growth stagnates. Several mechanisms have been identified to cause stagnation, such as boundary pinning by impurities, the presence of a boundary melt, or thin films between grains [4]. Experiments [12] have revealed an intermittent grain-boundary dynamics that

is hard to reconcile with the classical picture of uniform grain growth [13]. Based on molecular dynamics simulations [4], it has been argued that the grain-boundary roughness controls the boundary mobility, hence the overall grain growth, and that the presence of a small fraction of low-mobility, smooth grain boundaries can lead to stagnation. Grain rotation and grain coalescence due to a coupling between the normal growth and tangential motion have been recently suggested as important processes in the evolution of high-purity polycrystalline materials [8,9]. The experimental observations on grain rotation have been further backed by models reproducing the subdiffusive scaling behavior of grain growth dominated by grain rotation and coalescence [9].

In this Rapid Communication, we present numerical results on the anomalous coarsening dynamics of polycrystalline films and the influence of grain rotation. We use the phase-field crystal model that has been shown to be an efficient approach to modeling various aspects of polycrystalline dynamics on diffusive time scales [14–17]. We observe a transition between a dynamical state where grains continuously coarsen and a state where grain growth stagnates, with a crossover time that diverges as the quenching depth is lowered. Our setup consists of initial crystal seeds of random lattice orientations in a two-dimensional undercooled melt. The crystals are seeded at random sites chosen from a uniform distribution. At these sites we plant a small crystal seed, consisting of seven atoms in a hexagonal configuration with an angular orientation also chosen from a random uniform distribution. Without lack of generality, the system might as well be seeded by adding random noise to the initial density field of the undercooled melt. The latter approach would not change any of our results. During crystal growth, we track the lattice orientation and the area occupied by the individual grains. Figure 1 shows a few snapshots of polycrystalline textures during a coarsening process. At the early stages in the coarsening process, the mean grain area increases at a rate that depends on the quenching temperature. The grain growth continues on longer time scales only for shallow undercoolings below the melting temperature  $T_m$ , whereas it crosses over to a stagnation plateau when the melt is deeply quenched to temperatures much lower than  $T_m$ . The saturation value of the mean grain

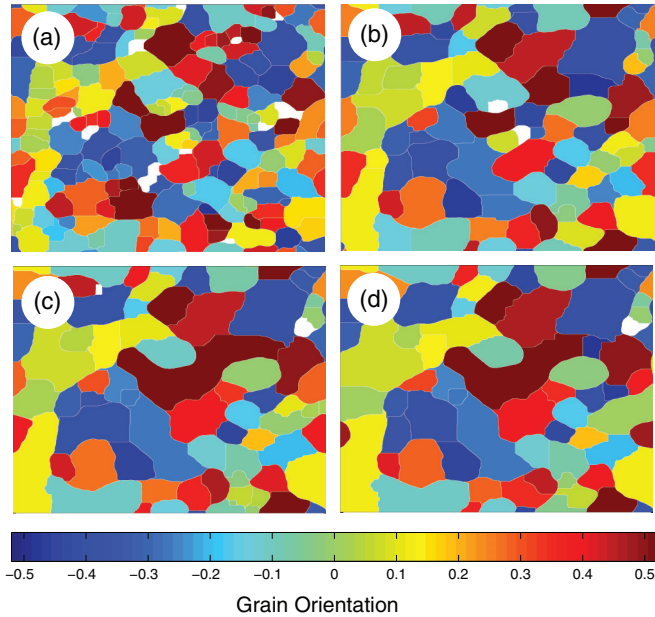


FIG. 1. (Color online) Time snapshots of grain growth in a polycrystalline material taken at simulation time steps (a)  $t = 400$ , (b)  $t = 12000$ , (c)  $t = 36000$ , and (d)  $t = 225000$ . The system size is 1024 by 1024, which corresponds to approximately 100 by 100 atom units, and the simulation has been run with the temperature controlling parameter set to  $a_2 = -0.05$  (corresponding to a relatively cold system). The individual grain colors denote the lattice orientation in radians. In the last frame the grain growth has reached a fixed state where even relatively high levels of thermal noise cannot reactivate grain-boundary migration or internal rearrangement.

area depends nontrivially on the quenching temperature [see Figs. 3 and 2(b)].

*The model.* The phase-field crystal (PFC) model operates on microscopic length scales and diffusive time scales, and thus constitutes an efficient computational alternative to traditional atomistic methods that are constrained on short time scales comparable to atomic vibrations. The PFC method has been applied to different nonequilibrium phenomena in (poly)crystalline materials including phase transitions [14,18], and elastic and plastic deformations [16,19]. The coarse-grained time resolution of the PFC method allows for an efficient modeling of slow dynamics of dissipative structures such as grain boundaries and crystal defects. In the simplest formulation, the evolution of the PFC density field  $\psi$  is governed by an overdamped, diffusive equation of motion on the form

$$\frac{\partial \psi}{\partial t} = \nabla^2 \frac{\delta \mathcal{F}[\psi; T]}{\delta \psi}, \quad (1)$$

where the static free-energy functional  $\mathcal{F}[\psi; T]$ , which determines the equilibrium properties of the crystal phase, has the phenomenological form of the Swift-Hohenberg free energy, but can also be derived from microscopic details using the density functional theory [14]. Here, we consider the free-energy functional as derived from the density functional theory for a hexagonal (fcc) crystal lattice in 2D and

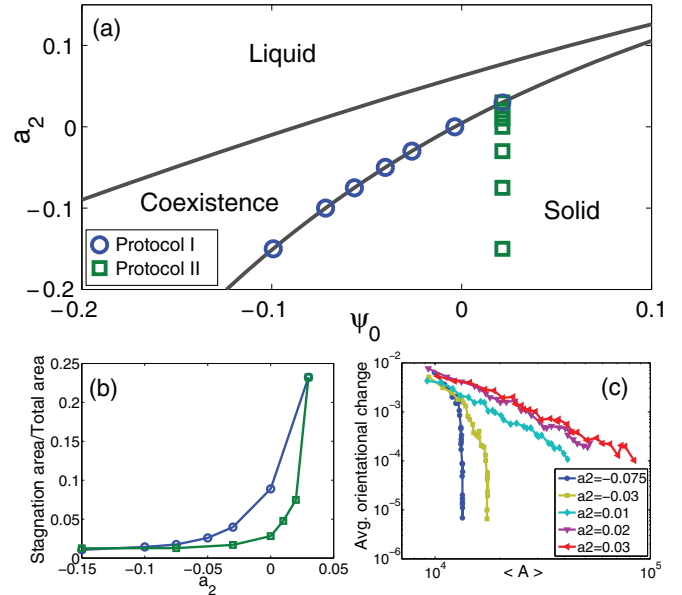


FIG. 2. (Color online) (a) shows a phase diagram with points indicating the two simulation protocols used. In protocol I, simulations were carried out along the coexistence line, and in protocol II, simulations were carried out for a fixed mean density  $\psi_0$ . The average grain area in the stagnated state for the two protocols is shown as a function of  $a_2$  in (b). We observe that for values of  $a_2$  approaching from below 0.03, the grain areas become of the order of the system size before growth stagnates. For simulations according to protocol II, the average change in grain orientation vs the average grain area is shown in (c). At low temperatures (low values of  $a_2$ ), grain rotation and grain growth quickly stagnates. Close to the melting temperature grain rotation goes down while the grain growth remains fast.

given as

$$\mathcal{F}[\psi; T] = \int d\mathbf{r} \left[ \frac{1}{2} \psi (\nabla^2 + 1)^2 \psi + \frac{a_2}{2} \psi^2 - \frac{1}{6} \psi^3 + \frac{1}{12} \psi^4 \right], \quad (2)$$

where the parameter  $a_2$  and the mean density  $\psi_0$  are related to the critical melting temperature  $T_m$  according to the phase diagram in Fig. 2(a). The phase diagram is computed by the one-mode approximation and common tangent construction. The local terms in Eq. (2) correspond to the coarse-grained free energy of an ideal gas, whereas the nonlocal term follows from the lowest-order gradient expansion of the interactions that allow for a periodic ground state corresponding to a triangular lattice in 2D.

Several extensions of Eq. (1) have been proposed by introducing additional time scales for faster acoustic relaxation of the elastic fields. The modified PFC model proposed in Ref. [16] is based on a two-time-scale dynamics of the PFC mimicked by a second-order time derivative of the  $\psi$  field, where the fast time scale resolves the rapid elastic relaxation. The fast dynamics related to phonons is taken into account by a three-time-scale dynamics of the PFC that can be derived from a generalized hydrodynamics of solids [20]. Since polycrystalline dynamics is a dissipative process, the fast elastic relaxation time scale does not influence the coarsening dynamics. Thus, for simplicity, we present numerical results obtained from the diffusive PFC given by Eq. (1), although

similar results were achieved from test simulations including elastic relaxations.

We solve numerically Eq. (1) using a pseudospectral method similar to that in Ref. [21], where time is propagated using an exponential time difference method. Simulations are carried out according to two protocols [see Fig. 2(a)], protocol I, where we follow the lower boundary of the solid-liquid coexistence region in the phase diagram, i.e., the crystal density and the parameter  $a_2$  are changed simultaneously, and protocol II, where the average density is fixed and the parameter  $a_2$  is varied. The parameter  $a_2$  is chosen in the range  $-0.15$  to  $0.03$ . For the simulations along the coexistence line, mean density  $\psi_0$  varies between  $-0.1$  and  $0.02$ .

The individual crystal orientations can be extracted from the phase-field crystal density by using a wavelet transformation [22]. Calculating the magnitude of the gradient in the grain orientation, we observe that the orientation changes most rapidly across grain boundaries. We can use this together with a watershed algorithm to identify individual grains (see Fig. 1).

*Results and discussion.* Polycrystalline microstructures, formed by grain nucleation and growth from an undercooled melt, initially coarsen with time at a rate depending on the quenching temperature. Figure 3 shows the average grain areas as functions of time for fixed crystal densities (i.e., according to simulation protocol II in the phase diagram). The late-stage evolution is characterized by a crossover to a grain-growth stagnation regime where the steady-state mean grain area increases as the quenching depth is decreased. We observe that the crossover time  $t_s$  depends nontrivially on the quenching temperature, such that its value diverges as  $T \rightarrow T_m$ . As long as the stagnation state is reached before

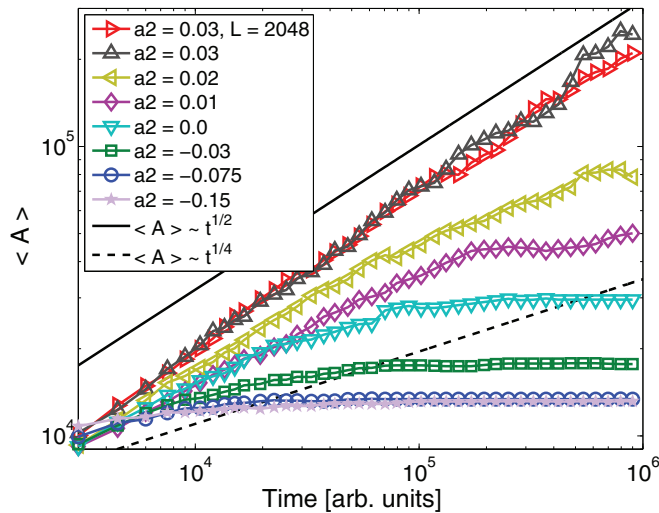


FIG. 3. (Color online) Mean grain size as a function of time for different quenching depths. We observe a transition from fast stagnation at large quenching depths (low values of  $a_2$ ) to a power-law scaling of grain size at shallow quenching depths (larger values of  $a_2$ ). In the latter case, i.e., for high temperatures, the scaling exponent is approximately  $\alpha = 1/2$ . Each line is averaged over five simulations of a system of size  $L = 1024$ . For  $a_2 = 0.03$ , we have further included simulations of a system of size  $L = 2048$ . Two lines corresponding to power laws with exponents  $1/4$  and  $1/2$  have been added as guides to the eye.

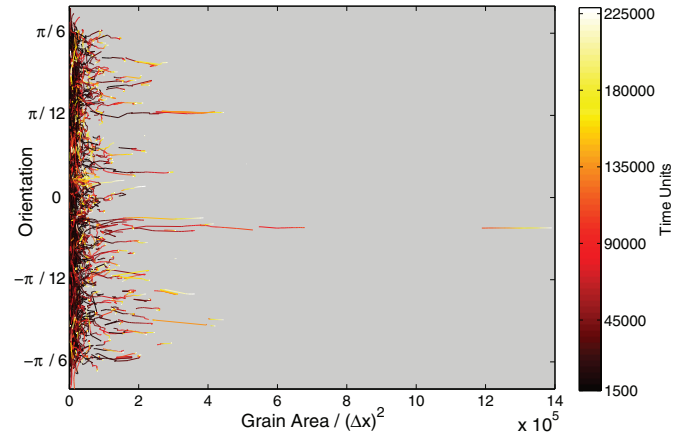


FIG. 4. (Color online) Individual grain trajectories in a lattice orientation and grain area diagram ( $a_2 = 0.03$ , protocols I and II). The areas of the individual grains have been normalized by the average size to a given time. The time evolution along the trajectories is indicated by the color legend. Note that the big grain separated from all the smaller grains is formed by consecutive alignment and merging of smaller grains.

the grain sizes become comparable to the system size, we have not observed a significant change in the average grain areas when varying the system size. In Fig. 2(b), we show for the two protocols the average grain size in the stagnated state (when there is no more dynamics) as  $a_2$  is increased. For simulation protocol II, we observe a rapid increase in the grain sizes before the coexistence line is crossed.

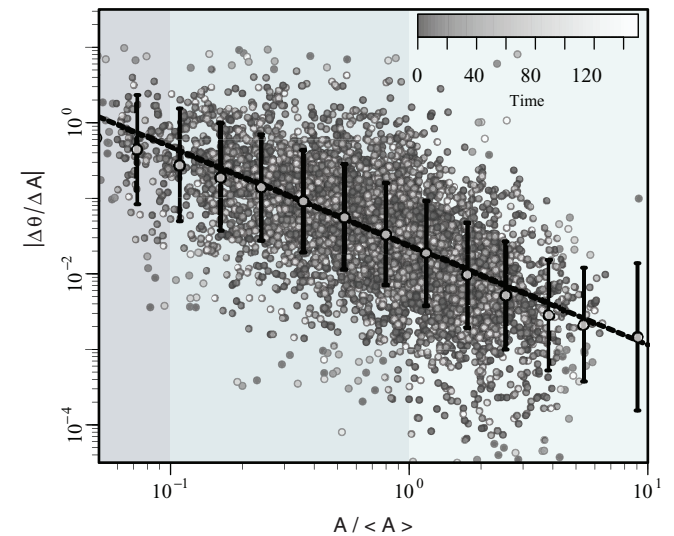


FIG. 5. (Color online) Grain rotation over area change  $|\Delta\theta/\Delta A|$  in a fixed time step  $\Delta t = 1500$  is shown as a function of the area divided by the mean area (at a given time step)  $A/\langle A \rangle$  ( $a_2 = 0.03$ ). We observe a systematic decrease in the rotation per area as the grain area is increased. The colors of the individual points, indicated by the color legend, represent the time at which a data point was observed. We note that there seems to be no clear difference in this plot between the early- and late-stage dynamics. The local average value of  $|\Delta\theta/\Delta A|$  is shown together with the sample variation (standard deviation), marked by error bars in black, and the line on top is a best fit with a power law. The best fit yields an exponent  $\beta = 1.25 \pm 0.06$ .

By tracking the angular evolution of the individual grains and their change in areas, we have considered in detail the correlation between the rotation rate and growth rate of the grains. In Fig. 4, we show the grain trajectories in the space of their misorientation and area size. We notice that at the early stages in the coarsening process, the small grains tend to follow a random meandering in the misorientation space, i.e., small grains rotate much more than bigger grains. However, in the later coarsening stage, the grain-boundary network is between large grains with selected misorientations. Also, we notice that some of the big grains suddenly disappear, which is an indication of coalescence where one grain rotates until its lattice orientation aligns with that of one of its neighbors. In Fig. 2(c), we observe that for low temperatures the grain stagnation is concomitant with a rapid decrease in grain rotation.

In general, the amount of grain rotation per change in area goes up for small grains (see Fig. 5). A best fit suggests, for relatively large areas, a scaling relation between the grain misorientation change and area change on the form

$$\left| \frac{\Delta\theta}{\Delta A} \right| \sim A^{-\beta}, \quad (3)$$

where the scaling exponent is estimated to be  $\beta = 1.25 \pm 0.06$  for  $a_2 = 0.03$ . If the grain rotation is solely due to the coupling to the normal motion, i.e.,  $r d\theta/dt = \Gamma v_n$ , the conservation of the number of dislocations along the grain boundary implies

that  $r(t)\theta(t) = \text{const}$ , or, equivalently,  $\theta(t) \sim A^{-1/2}(t)$  [8]. Consequently, it follows that  $\beta = 3/2$ . We ascribe the difference between the measured and predicted value of  $\beta$  to the variation in misorientation that a grain has in a polycrystalline matrix with its neighbors. At low quenching, the crystals are softer and the grain-boundary network more “greased,” allowing for sliding, dislocation reactions, or even premeltings. We have further performed simulations (not shown here) where we observe that in protocol I and for  $a_2 > 0.03$  most of the energy is dissipated in grain growth rather than grain rotation. Equivalently, grain rotation eventually stops when crossing from below the line to the solid-liquid coexistence region.

In summary, we have studied the anomalous coarsening and grain-growth stagnation in polycrystalline films using the phase-field crystal model. We find that the coarsening law is characterized by a power-law increase of the mean grain area for higher quenching temperatures, and for lower quenching temperatures we observe a temperature-dependent crossover to a stagnated state. This suggests that the subdiffusive coarsening law is non-universal, although the probability distribution of grain size has shown to be robust against temperature variations. Moreover, we observe that the late-stage coarsening is accompanied by a sudden decrease in grain rotation and a simultaneous stagnation.

*Acknowledgments.* This study was supported through a grant “Earth Patterns” by the Villum Foundation and by Physics of Geological Processes.

- 
- [1] J. von Neumann, in *Metal Interfaces*, edited by C. Herring (American Society for Metals, Cleveland, OH, 1952), p. 108.
  - [2] W. W. Mullins, *J. Appl. Phys.* **27**, 900 (1956).
  - [3] F. J. Humphreys and M. Hatherly, *Recrystallization and Related Annealing Phenomena*, Vol. 416 (Elsevier, Oxford, UK, 2004).
  - [4] E. A. Holm and S. M. Foiles, *Science* **328**, 1138 (2010).
  - [5] C. E. Krill, III, L. Helfen, D. Michels, H. Natter, A. Fitch, O. Masson, and R. Birringer, *Phys. Rev. Lett.* **86**, 842 (2001).
  - [6] C. Nichols, C. Mansuri, S. Townsend, and D. Smith, *Acta Metall. Mater.* **41**, 1861 (1993).
  - [7] K. Barmak, E. Eggeling, D. Kinderlehrer, R. Sharp, S. Ta'asan, A. Rollett, and K. Coffey, *Prog. Mater. Sci.* **58**, 987 (2013).
  - [8] J. W. Cahn and J. E. Taylor, *Acta Mater.* **52**, 4887 (2004).
  - [9] D. Moldovan, V. Yamakov, D. Wolf, and S. R. Phillpot, *Phys. Rev. Lett.* **89**, 206101 (2002).
  - [10] H. Frost, *Mater. Charact.* **32**, 257 (1994).
  - [11] E. De Achaval, O. Nasello, and E. Ceppi, *J. Phys. Colloq.* **48**, C1 (1987).
  - [12] S. Schmidt, S. Nielsen, C. Gundlach, L. Margulies, X. Huang, and D. J. Jensen, *Science* **305**, 229 (2004).
  - [13] R. D. MacPherson and D. J. Srolovitz, *Nature (London)* **446**, 1053 (2007).
  - [14] K. R. Elder, N. Provatas, J. Berry, P. Stefanovic, and M. Grant, *Phys. Rev. B* **75**, 064107 (2007).
  - [15] J. Mellenthin, A. Karma, and M. Plapp, *Phys. Rev. B* **78**, 184110 (2008).
  - [16] P. Stefanovic, M. Haataja, and N. Provatas, *Phys. Rev. Lett.* **96**, 225504 (2006).
  - [17] A. Adland, Y. Xu, and A. Karma, [arXiv:1303.0577](https://arxiv.org/abs/1303.0577).
  - [18] C. V. Achim, M. Karttunen, K. R. Elder, E. Granato, T. Al-Nissila, and S. C. Ying, *Phys. Rev. E* **74**, 021104 (2006).
  - [19] H. Emmerich, H. Löwen, R. Wittkowski, T. Gruhn, G. I. Tóth, G. Tegze, and L. Gránásy, *Adv. Phys.* **61**, 665 (2012).
  - [20] S. Majaniemi and M. Grant, *Phys. Rev. B* **75**, 054301 (2007).
  - [21] M. Cross, D. Meiron, and Y. Tu, *Chaos* **4**, 607 (1994).
  - [22] H. M. Singer and I. Singer, *Phys. Rev. E* **74**, 031103 (2006).